DMD Fast Forward. Published on June 20, 2011 as doi:10.1124/dmd.111.040675

Preclinical Species and Human Disposition of (1*S*,2*S*,3*S*,4*R*,5*S*)-5-[4-Chloro-3-(4-ethoxybenzyl)phenyl]-1-hydroxymethyl-6,8-dioxabicyclo[3.2.1]octane-2,3,4-triol (PF-04971729), a Selective Inhibitor of the Sodium-Dependent Glucose Cotransporter 2 (SGLT2) and Clinical Candidate for the Treatment of Type 2 Diabetes Mellitus

Amit S. Kalgutkar, Meera Tugnait, Tong Zhu, Emi Kimoto, Zhuang Miao, Vincent Mascitti, Xin Yang, Beijing Tan, Robert L. Walsky, Jonathan Chupka, Bo Feng and Ralph P. Robinson

Pharmacokinetics, Dynamics and Metabolism Department (A.S.K., M.T., T.Z., E.K., Z.M., X.Y., B.T., R.L.W., J.C., B.F.) and Worldwide Medicinal Chemistry (V.M., R.P.R), Pfizer Global Research and Development, Groton

DMD Fast Forward. Published on June 20, 2011 as DOI: 10.1124/dmd.111.040675
This article has not been copyedited and formatted. The final version may differ from this version.
DMD #40675

Running Title: Disposition of a Novel SGLT2 Inhibitor

Address correspondence to: Amit S. Kalgutkar, Pharmacokinetics, Dynamics, and Metabolism Department, Pfizer Global Research and Development, Groton, CT 06340. Phone: (860)-715-2433. E-mail: **amit.kalgutkar@pfizer.com**

Text Pages (including references): 25

Tables: 2

Figures: 8

References: 40

Abstract : 241

Introduction : 597

Discussion : 1104

Abbreviations used are: T2DM, type 2 diabetes; PF-04971729, (1*S*,2*S*,3*S*,4*R*,5*S*)-5-[4-Chloro-3-(4-ethoxybenzyl)phenyl]-1-hydroxymethyl-6,8-dioxabicyclo[3.2.1]octane-2,3,4-triol; P450, cytochrome P450; UGT, uridine glucuronosyl transferase; LC-MS/MS, liquid chromatography-tandem mass spectrometry; MRM, multiple reaction monitoring; p-gp, p-glycoprotein; BCRP, breast cancer resistance protein; CID, collision-induced dissociation; i.v., intravenous; p.o., oral; CL_p, plasma clearance; CL_b, blood clearance; CL/F, oral clearance; Vd_{ss}, steady state distribution volume; AUC, area under the plasma concentration/time curve; C_{max}, maximal plasma concentration after oral dosing; T_{max}, time to reach C_{max}; F, oral bioavailability; A, apical; B, basolateral; OCT, organic cation transporter; t_R, retention time; F_a, fraction absorbed.

DMD Fast Forward. Published on June 20, 2011 as DOI: 10.1124/dmd.111.040675
This article has not been copyedited and formatted. The final version may differ from this version.
DMD #40675

Abstract

(1*S*,2*S*,3*S*,4*R*,5*S*)-5-[4-Chloro-3-(4-ethoxybenzyl)phenyl]-1-hydroxymethyl-6,8-dioxabicyclo[3.2.1]octane-2,3,4-triol (PF-04971729), a potent and selective inhibitor of the sodium-dependent glucose cotransporter 2 (SGLT2), is currently in phase 2 trials for the treatment of diabetes mellitus. The paper describes the preclinical species and *in vitro* human disposition characteristics of PF-04971729, which were performed to support the first-in-human study. Plasma clearance was low in rats (4.04 ml/min/kg) and dogs (1.64 ml/min/kg) resulting in half-lives of 4.10 hours and 7.63 hours, respectively. Moderate to good bioavailability in rats (69 %) and dogs (94 %) was observed after oral dosing. The *in vitro* biotransformation profile of PF-04971729 in liver microsomes and cryopreserved hepatocytes from rat, dog and human was qualitatively similar; prominent metabolic pathways included mono-hydroxylation, *O*-deethylation and glucuronidation. No human-specific metabolites of PF-04971729 were detected in *in vitro* studies. Reaction phenotyping studies using recombinant enzymes indicated a role of CYP3A4/3A5, CYP2D6 and UGT1A9/2B7 in the metabolism of PF-04971729. No competitive or time-dependent inhibition of the major human cytochrome P450 enzymes was discerned with PF-04971729. Inhibitory effects against the organic cation transporter 2 mediated uptake of [^{14}C]-metformin by PF-04971729 also were very weak (IC_{50} ~ 900 μM). Single-species allometric scaling of rat pharmacokinetics of PF-04971729 was used to predict human clearance, distribution volume and oral bioavailability. Human pharmacokinetic predictions were consistent with the potential for a low daily dose. First-in-human studies following oral administration indicated that the human pharmacokinetics/dose predictions for PF-04971729 were in the range that is likely to yield a favorable pharmacodynamic response.

DMD Fast Forward. Published on June 20, 2011 as DOI: 10.1124/dmd.111.040675
This article has not been copyedited and formatted. The final version may differ from this version.

Introduction

Type 2 diabetes mellitus (T2DM), a chronic disease prevalent worldwide (King et al., 1998), is characterized by insulin resistance in muscle and liver, resulting in higher blood glucose levels. As blood glucose levels escalate, more insulin is required over time and with increasing severity of insulin resistance, hyperinsulinemia develops into insulin-deficiency as a result of progressive β-cell failure in the pancreas (DeFronzo, 1988 and 2009). Approximately 85% of patients with T2DM are obese or overweight, a key factor underlying the development and maintenance of insulin resistance (Mokdad et al., 2003). Individuals with T2DM have an increased risk of developing both microvascular (nephropathy, neuropathy, retinopathy) and macrovascular complications, and have an increased mortality rate from cardiovascular disease than adults who are not diabetic (Stratton et al., 2000).

In normal individuals, glucose filtered from the blood in the glomerulus is almost completely reabsorbed, such that <1% of glucose is excreted in urine. The low-affinity, high capacity sodium-dependent glucose cotransporter 2(SGLT2), expressed mainly in the S1/S2 segment of the proximal tubule of the nephron, is largely responsible for the reabsorption process (Kanai et al., 1994; Wallner et al., 2001). Although the high-affinity sodium-dependent glucose cotransporter 1 (SGLT1) is expressed to some extent in the kidney and contributes to glucose reabsorption, it is mainly expressed in the small intestine, where it plays a role in glucose absorption (Pajor and Wright, 1992; Wright, 2001).

It is now well-established that suppressing the activity of SGLT2 inhibits renal glucose reabsorption, thereby increasing the excretion of excess glucose from the body and assisting in the reduction of hyperglycemia in T2DM (Oku et al., 1999; Adachi et al., 2000; Zhang et al., 2005, 2006; Bołdys and Okopień 2009; Neumiller et al., 2010; Robinson et al., 2010). Due to

DMD Fast Forward. Published on June 20, 2011 as DOI: 10.1124/dmd.111.040675
This article has not been copyedited and formatted. The final version may differ from this version.

the insulin-independent mechanism of action, SGLT2 inhibitors are associated with a low risk for hypoglycemia (Katsuno et al., 2007; Fujimori et al., 2008; Wilding et al., 2009). Furthermore, there is the potential for clinically significant weight loss and reduced hepatic glucose production and amelioration of glucotoxicity (Abdul-Ghani and DeFronzo, 2008; Nair and Wilding, 2010).

Several SGLT2-selective inhibitors are in various stages of clinical trials (Sha et al., 2011; Aires and Calado, 2010; Nair and Wilding, 2010); proof-of-concept has been reported with dapagliflozin (Meng et al., 2008) in phase 2b studies in patient with type 2 diabetes (Kasichayanula et al., 2011; List et al., 2009). Results from a 24-week phase 3 clinical study with dapagliflozin have also demonstrated significant mean reductions in the primary endpoint, glycosylated hemoglobin levels, HbA1c, and in the secondary endpoint, fasting plasma glucose, when added to metformin in people with T2DM inadequately controlled with metformin alone (Bailey et al., 2010). The study also evaluated the potential impact of dapagliflozin on weight loss and demonstrated that individuals receiving dapagliflozin had statistically greater mean reductions in body weight compared with individuals taking placebo.

We recently disclosed a novel class of SGLT2 inhibitors bearing a unique dioxa-bicyclo[3.2.1]octane (bridged ketal), from which, (1*S*,2*S*,3*S*,4*R*,5*S*)-5-[4-Chloro-3-(4-ethoxybenzyl)phenyl]-1-hydroxymethyl-6,8-dioxabicyclo[3.2.1]octane-2,3,4-triol (PF-04971729) (Figure 1) emerged as a candidate for further advancement (Mascitti et al., 2011). PF-04971729 demonstrated > 2000-fold selectivity for SGLT2 inhibition (relative to SGLT1) *in vitro* and revealed a concentration-dependent glucosuria following oral administration to rats. In order to evaluate the potential for further clinical development and toxicological evaluations, preclinical pharmacokinetics and disposition of PF-04971729 were characterized in rats and dogs

and *in vitro* human hepatic tissue. Results from these studies were used to predict human pharmacokinetic parameters via allometric scaling approach. Preliminary assessments of PF-04971729 in the clinic suggest a fairly precise prediction of human pharmacokinetics, which should translate into a favorable pharmacodynamic response.

Materials and Methods

Materials. PF-04971729 and its *O*-deethylated phenol metabolite M1 (chemical and isomeric purity > 99% by HPLC and NMR) CP-100,356 and the selective cytochrome P450 (CYP) 2C19 inhibitor (+)-*N*-3-benzylnirvanol were synthesized at Pfizer Global Research and Development (Groton, CT, USA). NADPH was purchased from Sigma-Aldrich (Milwaukee, WI, USA). Probe CYP substrates (phenacetin, bupropion, amodiaquine, diclofenac, *S*-mephenytoin, dextromethorphan, felodipine, testosterone and midazolam) for individual CYP enzymes and recombinant human uridine glucuronosyl transferase (UGT) isoforms were purchased from BD Gentest (Bedford, MA). Recombinant human CYP isozymes were purchased from Invitrogen (Carlsbad, CA). Cryopreserved rat, dog and human hepatocytes were obtained from Celsis (Chicago, IL). Pooled human (pool of 50 livers from male/female), male Beagle dog, and male Sprague-Dawley rat liver microsomes were purchased from BD Gentest (Woburn, MA). [^{14}C]-Metformin (54 mCi/mmol) was obtained from Morvek Radiochemicals (Brea, CA). Solvents used for analysis were of analytical or HPLC grade (Fisher Scientific, Pittsburgh, PA, USA).

Plasma protein binding. The binding of PF-04971729 to rat, dog and human plasma proteins was determined using the equilibrium dialysis method (Pacifici and Viani 1992) using cellulose membranes (HTdialysis, Gales Ferry, CT) with a molecular weight cutoff of 12-14 kDa. For plasma protein binding studies, plasma was fortified with PF-04971729 at

concentrations of 2.3 and 23 μM, which reflects a theoretical plasma concentration anticipated in humans and a multiple thereof to assess saturation of plasma protein binding. The plasma samples (150 μl) were subjected to equilibrium dialysis (n = 3) against an equal volume of phosphate buffered saline (pH 7.4) at 37 °C with gentle shaking in a 95/5 O_2/CO_2 incubator. Following equilibration (~ 6 h), the volume of the plasma and buffer samples removed from each equilibration cell was noted. Aliquots of dialyzed plasma (20 μl) and buffer (100 μl) were transferred to 96-well blocks and acetonitrile (200 μl) containing an internal standard (molecular weight = 390, 250 ng/ml) was added to each well. Each matrix was normalized to the other by the addition of equal volumes of the opposite matrix, (i.e., plasma to buffer and buffer to plasma). Samples were then centrifuged at 3000 x *g* for 10 min; the supernatants were analyzed by liquid-chromatography tandem mass spectrometry (LC-MS/MS). Non-specific binding of PF-04971729 to the equilibrium dialysis device was minimal. The percentage of PF-04971729 bound to plasma proteins was calculated as: 100 – [(concentration of PF-04971729 in buffer/concentration of PF-04971729 in plasma) x 100].

Blood cell partitioning. Blood to plasma partitioning of PF-04971729 was determined in fresh rat, dog and human whole blood and plasma to which was added PF-04971729 to yield a final concentration of 2.3 μM (n= 3). Samples were incubated on a shaking water bath for 120 min at 37 °C. Post-incubation, whole blood samples were centrifuged at 3000 x *g* to obtain plasma. Aliquots (50 μl) of plasma sample incubations and plasma isolated from whole blood were mixed with acetonitrile (200 μl) containing an internal standard (molecular weight = 390, 500 ng/ml) and centrifuged. Supernatants were analyzed using LC-MS/MS. A blood/plasma partitioning ratio for PF-04971729 was calculated from the concentrations in blood and plasma.

DMD Fast Forward. Published on June 20, 2011 as DOI: 10.1124/dmd.111.040675
This article has not been copyedited and formatted. The final version may differ from this version.

CYP inhibition studies. *Competitive inhibition.* Standard marker substrates of CYP isozymes were incubated with pooled human liver microsomes in the presence of NADPH (1.3 mM) in 100 mM KH_2PO_4, pH 7.4 containing 3.3 mM $MgCl_2$ at 37 ^oC open to air. The incubation volume was 0.2 ml. Microsomal protein concentrations, substrate concentrations, incubation times and reaction termination solvents for each activity have been described in detail previously (Walsky and Obach, 2004). Probe substrate concentrations utilized were near K_M values that had been previously determined and incubation times were selected based on previous determinations of reaction velocity linearity (Walsky and Obach, 2004). Incubation mixtures contained PF-04971729 at concentrations of 0, 0.0952, 0.301, 0.951, 3.00, 9.49, and 30 μM. Stock solutions of PF-04971729 were prepared in 95:5 acetonitrile:water. Incubations were commenced with the addition of NADPH. *Time-dependent inhibition.* Pooled human liver microsomes (protein concentration = 0.1 – 1.0 mg/ml, depending on which isozyme was assessed) were preincubated with PF-04971729 at a concentration of 300 μM, in 100 mM KH_2PO_4, pH 7.4 containing 3.3 mM $MgCl_2$ at 37 ^oC open to air in the presence and absence of NADPH (1.3 mM). Preincubations were carried out for 30 minutes at 37 ^oC. After preincubation, a portion of the incubation mixture (20 μl) was added to a mixture containing a probe CYP isozyme substrate (concentration ~ K_M) (Walsky and Obach, 2004) in 100 mM KH_2PO_4, pH 7.4 containing 3.3 mM $MgCl_2$ and NADPH (1.3 mM) at 37 ^oC. The final incubation volume was 0.2 ml. At the end of the incubation period, acetonitrile containing internal standard was added and the mixture was filtered using a Millipore Multiscreen HA filter plate to remove microsomal protein. Filtered solutions were analyzed by LC-MS/MS using a Micromass Ultima tandem quadrupole mass spectrometer (Waters Corporation, Milford, MA) fitted with an electrospray interface. The HPLC system consisted of a Shimadzu SCL-10Avp

DMD Fast Forward. Published on June 20, 2011 as DOI: 10.1124/dmd.111.040675
This article has not been copyedited and formatted. The final version may differ from this version.

controller with LC-10ADvp pumps and CTC Analytics Leap autosampler. Metabolites of probe CYP substrates were analyzed using validated bioanalytical conditions established previously (Walsky and Obach, 2004). IC_{50} values for inhibition of CYP isozymes were estimated using the Sigma Plot curve-fitting software (SYSTAT Inc. San Jose, Ca.).

Human organic cation transporter 2 (hOCT2) inhibition studies. Human embryonic kidney 293 cells transfected with hOCT2 were obtained from Prof. Kathleen M. Giacomini (University of California, San Francisco). hOCT2 was subcloned into the mammalian expression vector pcDNA5/FRT and transfected into HEK293 flip-in® cells (Invitrogen Carlsbad, CA). Non transfected human embryonic kidney 293 cells were grown in Dulbecco's Modified Eagle Medium, 10% v/v heat inactivated fetal bovine serum, 1% v/v Penicillin/Streptomycin and 100 μg/ml Zeocin. Stably transfected hOCT2 cells were grown in Dulbecco's Modified Eagle Medium containing 10% fetal bovine serum, 1% gentamicin and 50 μg/ml Hygromycin B. hOCT2 assays were carried out in 24-well poly-D-lysine coated plates (Biocoat, Horsham, PA). Cells were seeded to reach confluence (80-100%) 48-72 h prior to each experiment. Immediately before the experiment, cells were placed on a 37 °C heat block and were washed twice with 1 ml Hank's balanced salt solution, pH 7.4 pre-warmed to 37 °C. After a 5 min acclimation period, the cells were incubated with 150 μl Hank's balanced salt solution buffer containing [^{14}C]-metformin (5 μM). In order to increase assay sensitivity, the metformin concentration chosen for the inhibition study was below its reported Km value (Bachmakov et al., 2009). Thus, the uptake of metformin at the concentration of 5 μM in the HEK293 cells transfected with hOCT2 is ten-fold greater than the corresponding uptake in wildtype HEK293 cells, which provides a large dynamic window to assess inhibitory potency against the cation transporter. After five minutes at 37 °C, the cellular uptake was terminated by washing the cells

three times with 1 ml ice-cold Hank's balanced salt solution. The cells were lysed in 400 µl 1% sodium dodecyl sulfate in Dulbecco's Phosphate-Buffered Saline buffer. The cells were covered and shaken for 10-15 minutes at room temperature. Accumulated radioactivity was determined by combining all of the cell lysate solution with 6.6 ml of scintillation fluid and mixed until homogenous. Radioactivity in each sample was determined by liquid scintillation counting on a Packard Tri-Carb 2900TR (Waltham, MA) scintillation counter and recorded as disintegrations per minute. The IC_{50} value for hOCT2 inhibition was determined in incubations with seven different concentrations of PF-04971729 ranging from 1.4 to 1000 µM (n = 3). Stock solutions of PF-04971729 were prepared in DMSO. hOCT2 inhibitor quinidine (1 mM) was used as a positive control (Zolk et al., 2009). Incubations were performed in 24-well culture plates using [^{14}C]-metformin (5 µM) spiked with PF-04971729 and applied simultaneously to the cells. The mean and standard deviation of substrate uptake rate were calculated for each sample. These values were then converted to % uptake relative to the control (substrate uptake without inhibitor), with the control representing 100% uptake. The IC_{50} value for PF-04971729 was estimated from a semi-logarithmic plot of concentrations versus percentage of net uptake relative to the control.

Caco-2 cell permeability. Caco-2 cells, obtained from the American Type Culture Collection (Rockville, MD), were seeded in 24-well Falcon Multiwell plates (polyethylene terephthalate membranes, pore size 1.0 µM) at 4.0 x 10^4 cells per well. The permeability studies on PF-04971729 at a concentration of 1 µM were conducted using a previously published protocol (Frederick et al., 2009). Studies were conducted in the presence or absence of the dual p-glycoprotein (p-gp) / breast cancer resistance protein (BCRP) inhibitor CP-100,356 (10 µM) to

both the apical and the basolateral compartments in the bidirectional permeability determination (Kalgutkar et al., 2009).

Animal pharmacokinetic studies. All animal care and *in vivo* procedures conducted were in accordance with guidelines of the Pfizer Animal Care and Use Committee. Male Sprague-Dawley rats (0.31 – 0.36 kg) and male Beagle dogs (9.4 – 11.6 kg) were used as animal models for allometric scaling of human pharmacokinetics. For oral (p.o.) pharmacokinetic studies, animals were fasted overnight before dosing whereas access to water was provided *ad libitum.* PF-04971729 was administered intravenously (i.v.) via the jugular vein of rats (n = 2) or the cephalic vein for dogs (n = 2). For p.o. studies, PF-04971729 was administered as the L-pyroglutamate co-crystal by oral gavage to rats (n = 3) and dogs (n = 3). PF-04971729 was administered at 2.0 mg/kg i.v. dose and 5.0 mg/kg p.o. dose in rats and at a 2.0 mg/kg dose for the i.v. and p.o. studies in dogs. Animals were fed following collection of the 4 hour blood samples. PF-04971729 was formulated as a solution in DMSO/polyethylene glycol 400/30% sulfobutylether-β-cyclodextrin (10/30/60, v/v/v) and 0.5% (w/v) methylcellulose with 10% (v/v) polyethylene glycol 400 for rat i.v. and p.o. studies, respectively. For assessment of dog i.v. and p.o. pharmacokinetics, PF-04971729 was formulated as a solution in 5% polyethylene glycol 400 in 23% hydroxypropyl-β-cyclodextrin and 0.5% (w/v) methylcellulose with 10% (v/v) polyethylene glycol 400, respectively. After dosing, serial plasma samples were collected at appropriate times and kept frozen at – 20 ^{o}C until LC-MS/MS analysis. Urine samples (0 – 7.0 and 7.0 – 24 h) were also collected after i.v. administration to rats and dogs.

Pharmacokinetic parameter generation in preclinical species. Plasma concentration versus time profile was generated for each animal. Standard non-compartmental pharmacokinetic analysis was performed using Watson Bioanalytical LIMS version 72003

(Thermo Electron Corporation, San Antonio, Texas) to determine plasma clearance (CL_p) and volume of distribution at steady state (Vd_{ss}). CL_p was calculated as the i.v. dose divided by the area under the plasma concentration-time curve from zero to infinity ($AUC_{0-\infty}$). $AUC_{0-\infty}$ was calculated by the linear trapezoid rule. The terminal slope of the ln (concentration) versus time plot was calculated by linear least-squares regression and the half-life was calculated as 0.693 divided by the absolute value of the slope. The maximum plasma concentration (C_{max}) observed after p.o. dosing and the time at which it was observed (T_{max}) were determined directly from the individual plasma concentration-time profiles. The absolute bioavailability (F) of the p.o. doses was calculated by using the following equation: $F = AUC_{0-\infty}^{p.o.} / AUC_{0-\infty}^{i.v.} \times Dose^{i.v.} / Dose^{p.o.}$

Bioanalytical methodology. Mass spectrometry was performed on a Sciex API4000 system equipped with a turbo-ionspray source (Applied Biosystems, Foster City, CA, USA) operated in negative ion mode. HPLC analysis was conducted on Shimadzu 10ADvp Binary HPLC system (Shimadzu Scientific Instruments Columbia, MD, USA) with a CTC-PAL (Thermo Scientific, Franklin, MA, USA) as the autosampler. Chromatographic separations were performed on a Phenomenex Synergy Max-RP 2 x 50mm 4 µ HPLC column (Torrance, CA, USA) using mobile phase A (10 mM ammonium acetate and 1% isopropyl alcohol in water) and mobile phase B (acetonitrile). A linear gradient from 5% B to 95% B over 1.5 min with the flow rate of 0.3 ml/min was performed to elute PF-04971729 and the internal standard. Analyst (version 1.4.1, Applied Biosystems, Foster City, CA, USA) was employed to control the instrument operation and acquire data in multiple reaction monitoring (MRM) mode. The ion transition for PF-04971729 was 435 → 303, and for the internal standard is 391 → 313. The dynamic range of the assay ranged from 5 ng/ml to 5000 ng/ml using linear regression with a weighting of $1/x^2$.

DMD Fast Forward. Published on June 20, 2011 as DOI: 10.1124/dmd.111.040675
This article has not been copyedited and formatted. The final version may differ from this version.

Pharmacokinetic projections to human. Single species allometric method was used to predict human pharmacokinetic parameters of PF-04971729. CL_p and Vd_{ss} observed in rats were corrected for species differences in protein binding and then scaled to humans according to equations 1 and 2 below (Frederick et al., 2009). This approach employs a fixed allometric exponent of 0.75 and 1.0 for clearance and volume, respectively. BW is the body weight (kg) (assumed to be 70 for human) and for rat actual body weight of animals (0.314, 0.361) in the study was used).

$$(1)\ \mathbf{CL_{human}} = \mathbf{CL_{animal}} \times \left(\frac{\mathbf{BW_{human}}}{\mathbf{BW_{animal}}} \right)^{\mathbf{0.75}}$$

$$(2)\ \mathbf{Vdss_{human}} = \mathbf{Vdss_{animal}} \times \left(\frac{\mathbf{BW_{human}}}{\mathbf{BW_{animal}}} \right)^{\mathbf{1.0}}$$

Human pharmacokinetic predictions assumed a simple one-compartment pharmacokinetic model with first order absorption. As such, human half-life was predicted according to equation 3 below.

$$(3)\ \mathbf{t1/2_{human}} = \frac{\mathbf{ln(2)} \times \mathbf{Vdss_{human}}}{\mathbf{CL_{human}}}$$

Metabolite identification. *Liver microsomes and recombinant CYP enzymes.* Stock solutions of PF-04971729 were prepared in methanol. The final concentration of methanol in the incubation media was 0.2% (v/v). Incubations were carried out at 37 ^{0}C for 60 min in a shaking water bath. The incubation volume was 1 ml and consisted of the following: 0.1 M potassium phosphate buffer (pH 7.4), liver microsomes from rat, dog and human (P450 concentration = 0.5 μM) or recombinant CYP isoforms (50 pmol of CYP 1A2, 2C9, 2C19, 2D6, 2E1, 3A4 and 3A5),

DMD Fast Forward. Published on June 20, 2011 as DOI: 10.1124/dmd.111.040675
This article has not been copyedited and formatted. The final version may differ from this version.

NADPH (1.0 mM) and PF-04971729 (10 – 20 μM). The reaction mixture was prewarmed at 37 °C for 2 min before adding NADPH. Incubations that lacked NADPH served as negative controls, and reactions were terminated by the addition of ice-cold acetonitrile (4 ml). The solutions were centrifuged (3,000 x *g*, 15 min) and the supernatants were dried under a steady nitrogen stream. The residue was reconstituted with 25% aqueous acetonitrile (250 μl) and analyzed for metabolite formation by LC-MS/MS.

Recombinant UGT enzymes. PF-04971729 (20 μM) was incubated with 10 human recombinant UGT isoforms (UGT1A1, 1A3, 1A4, 1A6, 1A8, 1A9, 1A10, 2B4, 2B7 and 2B15) for 40 min. The incubation was carried out at protein concentration of 0.5 mg/ml. The reaction mixture contained UDPGA (1mM), $MgCl_2$ (10 mM), and alamethicin (25 μg/ml). Reactions were terminated by adding acetonitrile to the incubation mixture at the ratio of 1:4. The residue was reconstituted with 25% aqueous acetonitrile (250 μl) and analyzed for metabolite formation by LC-MS/MS.

Cryopreserved hepatocytes. Cryopreserved rat (male Sprague-Dawley, pool of 15-20 livers), dog (pool of 4-8 male livers) or human (pool of three livers, one female and two males) hepatocytes were thawed and suspended in Williams' E media supplemented with 24 mM $NaHCO_3$ and 10% fetal bovine serum at 2×10^6 viable cells per ml. PF-04971729 (10 μM) was incubated with hepatocytes at 37 °C for 4 h with gentle agitation. A gas mixture of O_2/CO_2 (95:5) maintained at ~2.5 kPa for ~5 s was passed through this mixture at every hour of incubation. Flasks were corked immediately after gassing. Reactions were stopped by adding ice-cold acetonitrile (10 ml) and centrifuged (3000 x g, 15 min). The supernatants were dried under a steady stream of nitrogen and reconstituted with 25% aqueous acetonitrile (250 μl) and analyzed by LC-MS/MS for metabolite formation.

DMD Fast Forward. Published on June 20, 2011 as DOI: 10.1124/dmd.111.040675
This article has not been copyedited and formatted. The final version may differ from this version.

Bioanalytical methodology for metabolite identification. Qualitative assessment of the metabolism of PF-04971729 was conducted using a Thermo LTQ or LTQ-Orbitrap mass spectrometer (Thermo Electron, San Jose, CA) operated with a electrospray source and coupled to a Thermo Separations spectromonitor 3200 UV. The monitoring wavelength was 254 nm. Analytes were chromatographically separated using an HPLC system, which comprised of a HP-1050 solvent delivery system, HP-1050 membrane degasser and an HP-1050 autoinjector (Hewlett Packard, Palo Alto, CA). The autoinjector was programmed to inject 50 µl of sample onto a Synergi Fusion (Phenomenex) C-18 column, 250 x 4.6 mm 5 µm column using a gradient consisting of a mixture of 5 mM ammonium formate (pH 3.0) (solvent A) and acetonitrile (solvent B) at a flow rate of 1 ml/min. The binary gradient was as follows: solvent A to solvent B ratio was held at 95:5 (v/v) for 3 min and then adjusted to 55:45 (v/v) from 0 – 35 min, 30:70 (v/v) 35 – 45 min, 5:95 (v/v) 45 – 52 min where it was held for 3 min then returned to 95:5 (v/v) for 6 min before next analytical run. Postcolumn flow was split such that mobile phase was introduced into the mass spectrometer via an ion spray interface at a rate of 50 µl/min. The remaining flow was diverted to the UV detector positioned in line to provide simultaneous UV detection (λ = 254 nm) and total ion chromatogram. The mass spectrometer was operated in the positive ion mode and the interface was set at a spray voltage 4.5 kV. The scan event cycle used a full scan mass spectrum at unit resolution (LTQ) or at 30,000 resolution (Fourier transform). The exact mass measurement was based on external calibration performed on the same day. Initial full scans were performed between *m/z* 50 to 1000. PF-04971729 and its identifiable metabolites eluted in the first 30 min. Metabolites were identified in the full scan mode (from *m/z* 100 to 850) by comparing t = 0 samples to t = 40 – 60 (liver microsomes) / t = 240 min (hepatocytes) samples or through comparison with synthetic standard(s), and structural

information was generated from the collision-induced dissociation (CID) spectra of the molecular ions (MH^+). Due to the lack of nitrogen atoms and/or other positively charged sites in the structural architecture of PF-04971729, CID spectra of parent and metabolites were attained from the corresponding ammonium adducts and structure elucidation was based on these adducts.

Clinical pharmacokinetic data. The pharmacokinetics of PF-04971729 was evaluated in healthy volunteer subjects in a randomized, placebo-controlled, ascending single oral dose, crossover study over the dose range of 0.5 – 300 mg. The protocol was reviewed and approved by an independent ethics committee and all subjects gave written informed consent. There were two cohorts in the study with 12 healthy volunteers per cohort. Subjects in Cohort 1 received two single doses of PF-04971729 and one placebo dose in random order; in addition, one dose of PF-04971729 was administered in the fed state. Subjects in Cohort 2 received two single doses of PF-04971729 and one dose of placebo in a random order. Subjects were healthy volunteers aged 18-55 years and females participating in this study were of non-childbearing potential.

Results

Plasma Protein Binding. The extent of *in vitro* binding of PF-04971729 to plasma proteins was evaluated by equilibrium dialysis in rat, dog and human plasma . The mean percentages ± S.D. of plasma protein binding of PF-04971729 at concentrations of 2.3 and 23 μM were 96.0 ± 0.4 and 96.4 ± 0.5 (rat), 96.8 ± 0.02 and 96.8 ± 0.1 (dog) and 93.6 ± 0.1 and 94.7 ± 0.3 (human). These results show that PF-04971729 is highly bound to plasma proteins among the species examined, and binding is independent of concentration. PF-04971729 was stable in rat, dog and human plasma for > 6 hours at 37 ^{0}C at the concentrations utilized in the plasma free fraction determination.

DMD Fast Forward. Published on June 20, 2011 as DOI: 10.1124/dmd.111.040675
This article has not been copyedited and formatted. The final version may differ from this version.

Blood Cell Partitioning. The blood/plasma ratios for PF-04971729 were estimated to be 0.66 ± 0.01, 0.58 ± 0.02, and 0.66 ± 0.07 in rat, dog, and human, respectively, suggesting that PF-04971729 preferentially distributed into plasma over red blood cells.

Human CYP Isozyme Inhibition. PF-04971729 exhibited no relevant reversible and time-dependent inhibitory effects against CYP1A2, CYP2B6, CYP2C8, CYP2C9, CYP2C19, CYP2D6, or CYP3A4/5 (felodipine oxidase, midazolam-1'-hydroxylase, testosterone-6β-hydroxylase) activities. IC_{50} values could not be calculated since PF-04971729 did not inhibit any CYP activity more than 40% at the highest concentration tested. Under the present experimental conditions, known CYP isozyme-specific inhibitors furafylline, clopidogrel, montelukast, sulfaphenazole, (+)-*N*-3-benzylnirvanol, quinidine and ketoconazole demonstrated potent competitive inhibition of CYP1A2, 2B6, 2C8, 2C9, 2C19, 2D6 and 3A4 activity, respectively, in human liver microsomes (data not shown).

Inhibition of hOCT2 by PF-04971729. PF-04971729, at a concentration range of 1.4 – 1000 μM, was evaluated as a inhibitor of the hOCT2 transporter. The calculated IC_{50} for inhibition of hOCT2-mediated uptake of [^{14}C]-metformin by PF-04971729 was 917 μM (Figure 2). Under these experimental conditions, positive control quinidine (1 mM) (Zolk et al., 2009) inhibited > 80% [^{14}C]-metformin uptake mediated by hOCT2 (data not shown).

Caco-2 Permeability. The permeability coefficient of PF-04971729 across Caco-2 cells in the apical (A) to basolateral (B) direction was 4.1 x 10^{-6} cm/sec, a value that is comparable to drugs that exhibit moderate to good oral absorption in humans (Elsby et al., 2008). Under identical experimental conditions, the B to A permeability coefficient of PF-04971729 was 8.6 x 10^{-6} cm/sec (BA/AB ratio of 2.1). The presence of the dual P-gp/BCRP inhibitor CP-100,356 (Kalgutkar et al., 2009) did not greatly increase the absorptive permeability (4.7×10^{-6} cm/sec) of

DMD Fast Forward. Published on June 20, 2011 as DOI: 10.1124/dmd.111.040675
This article has not been copyedited and formatted. The final version may differ from this version.

PF-04971729. Thus, P-gp and BCRP do not appear to be limiting factors for oral absorption of PF-04971729.

Pharmacokinetics of PF-04971729 After Single Doses in Rats and Dogs. The pharmacokinetic parameters describing the disposition of PF-04971729 after i.v. and p.o. administration in preclinical species is shown in Table 1, and mean plasma concentration versus time profiles are depicted in Figure 3. Following an i.v. dose of 2.0 mg/kg, PF-04971729 exhibited a low blood clearance (CL_b) of 6.12 mL/min/kg (obtained by dividing the CL_p of 4.04 ml/min/kg by the blood to plasma ratio of 0.66), which is ~ 6 % of rat hepatic blood flow of 70 ml/min/kg). The Vd_{ss} was moderate (1.13 l/kg) compared with 0.6 l/kg for total body water in the rat, indicating extravascular distribution. The mean elimination half-life ($T_{1/2}$) was estimated to be 4.10 h. The percent of unchanged PF-04971729 excreted over a 24 h period in the urine was 27.5 %. Following p.o. administration of PF-04971729 as a L-pyroglutamic acid co-crystal at 5.0 mg/kg, systemic exposure of PF-04971729 as ascertained from C_{max} and AUC_{0-24} was 1940 ± 185 ng/ml and 14700 ± 4320 ng-hr/ml, respectively. The time to reach peak concentrations (T_{max}) was 1.0 h. The oral bioavailability (F) of PF-04971729 was 69%.

In the dog, following a i.v. dose of 2.0 mg/kg, PF-04971729 exhibited a low CL_p (1.64 ml/min/kg) / CL_b (2.83 ml/min/kg; ~ 8% of dog hepatic blood flow of 35 ml/min/kg) and a Vd_{ss} (0.83 l/kg) similar to total body water in the dog (0.6 l/kg), indicative of modest extravascular distribution in this species. The mean elimination $T_{1/2}$ was estimated to be 7.63 h. The percent of unchanged PF-04971729 excreted over a 24 h period in the urine was 2.0 %. Following p.o. administration of PF-04971729 as a L-pyroglutamic acid co-crystal to dogs at 2.0 mg/kg, mean systemic exposure of PF-04971729 as ascertained from C_{max} and $AUC_{0-\infty}$ was 2500 ± 215 ng/ml

DMD Fast Forward. Published on June 20, 2011 as DOI: 10.1124/dmd.111.040675
This article has not been copyedited and formatted. The final version may differ from this version.

and 19100 ± 3650 ng-hr/ml, respectively. The time to reach C_{max} was 0.83 ± 0.29 h. The mean *F* was 94%.

***In Vitro* Metabolic Profile.** *Liver Microsomes.* Figure 4 depicts the extracted ion chromatograms of incubation mixtures of PF-04971729 in NADPH-supplemented liver microsomes from rat, dog and human. PF-04971729 was the major peak in all microsomal incubations and there were no human-unique metabolites. Four metabolites (labeled M1, M2, M3, M4) of PF-04971729 were detected in liver microsomes from rat, dog and human at the retention times (t_R) noted in Table 2. M7 was a rat-specific metabolite. M1 – M4 and M7 were not detected when NADPH was omitted from the microsomal incubations suggesting that CYP isozymes catalyzed the rate-limiting step in their formation. PF-04971729 exhibited an ammonium adduct $(M+NH_4)^+$, which possessed an exact mass of 454.1632 (see Table 2 and Figure 5). Theoretical exact masses for the proposed fragment ion structures for m/z 329, 273, 207 and 135 in the CID spectrum of PF-04971729 (Figure 5) were consistent with the observed accurate masses (< 2 ppm difference). MS/MS data, proposed fragmentation patterns and structures for the metabolites of PF-04971729 are shown in table 2 and Figure 6, respectively. M1 possessed an exact mass of 470.1580 $((M + NH_4)^+$, an addition of 16 Da to the molecular weight of PF-04971729), which suggested that it was a mono-hydroxylated derivative of PF-04971729. The CID spectra showed diagnostic fragments at m/z 435, 407, 299 and 243. The ion at m/z 435 was due to the sequential loss of NH_3 and H_2O. The most abundant fragment ion, which occurred at m/z 407 (loss of 28 Da from m/z 435) was derived from the loss of ethylene unit. The absence of fragment ions derived from benzylic cleavage (e.g., m/z 207 and 135 seen in the mass spectrum of PF-04971729) in the CID spectrum of M1 suggested the benzylic position as the most likely site of hydroxylation. A proposed structure for M1 that is consistent

DMD Fast Forward. Published on June 20, 2011 as DOI: 10.1124/dmd.111.040675
This article has not been copyedited and formatted. The final version may differ from this version.

with the observed fragment ions is depicted in Figure 6. Metabolite M2 possessed a molecular ion at 426.1320 ($(M + NH_4)^+$, a loss of 28 Da from the molecular weight of PF-04971729); the CID spectrum and t_R was identical to the synthetic standard of the *O*-deethylated phenol metabolite of PF-04971729 (Figure 6). Like M1, metabolites M3 and M4 ($(M + NH_4)^+$ = 470.15) were derived from mono-hydroxylation of PF-04971729. A common fragment ion at m/z 207 in the mass spectrum of M3 and PF-04971729 suggested that the chlorobenzyl group was unaltered. The ions at m/z 123 and 151, which are 16 Da higher than the characteristic ions at m/z 107 and 135 in PF-04971729, suggested that the hydroxylation in M3 occurred on the ethoxyphenyl ring; a proposed structure that is consistent with the fragmentation pattern is depicted in Figure 6. In the case of M4, the CID spectrum showed fragment ions at m/z 435, 417, 399, 329, 207 and 135. The ion at m/z 435 resulted from sequential loss of NH_3 and H_2O, whereas, the ion at m/z 207 indicated that chlorophenyl moiety was unchanged. Based on these data, a tentative structure for M4 is shown in Figure 6. Rat-specific metabolite M7 showed an ammonia adduct ion $[M+NH_4]^+$ at m/z 442.12, which is 12 Da lower than parent compound and 16 Da higher than M2. This observation suggested that M7 was a mono-hydroxylated derivative of M2. The fragment ion at m/z 407 in the CID spectrum of M7 resulted from sequential loss of NH_3 and H_2O. Lack of ions that resulted from the characteristic benzylic cleavage seen in PF-04971729 suggested that the site of oxidation was the benzylic position in M2. A proposed structure for M7 is shown in Figure 6.

Cryopreserved Hepatocytes. Figure 7 depicts the extracted ion chromatograms of incubation mixtures of PF-04971729 in cryopreserved hepatocytes from rat, dog and human. PF-04971729 was the major peak in all hepatocyte incubations and there were no human-unique metabolites. Apart from the formation of oxidative metabolites M1 – M4 and M7, metabolites (M5a, M5b,

DMD Fast Forward. Published on June 20, 2011 as DOI: 10.1124/dmd.111.040675
This article has not been copyedited and formatted. The final version may differ from this version.

M5c, M6a, M6b, M6c and M8) derived from the glucuronidation of PF-04971729 and its oxidative metabolites were also observed in hepatocyte incubations. Metabolites M5a, M5b and M5c were regioisomers that displayed identical ammonia adduct ions $[M+NH_4]^+$ at m/z 630, 176 Da higher than PF-04971729, suggesting that they were obtained from glucuronidation of the glycoside hydroxyl groups (Figure 6). Metabolites M6a, M6b and M6c also were regioisomers that displayed identical ammonia adduct ions $[M+NH_4]^+$ at m/z 602, suggesting that they were obtained from glucuronidation of M2. The CID spectra showed fragment ions at m/z 459, 409, 391, 301, 283, 207 and 107. The ion at m/z 409 resulted from loss of glucuronic acid and NH_3 components, while the ion m/z 207 indicated the integrity of the chlorophenyl moiety. Proposed structures of M6a, M6b and M6c, which are consistent with the fragmentation pattern, are shown in Figure 6. M8 showed an ammonia adduct ion $[M+NH_4]^+$ at m/z 646, 192 Da higher than the molecular weight of PF-04971729, suggesting that M8 was a glucuronide conjugate of a mono-hydroxylated metabolite of PF-04971729. The MS^2 and MS^3 spectra of M8 showed fragment ions at m/z 470, 453, 435, 345, 207, 151, 139 and 123. The ions at m/z 470 and m/z 453 resulted from loss of the components of glucuronic acid (176 Da) and NH_3, respectively. The diagnostic ion at m/z 207, also observed in PF-04971729, suggested that chlorophenyl moiety was unaltered in M8. The MS^4 spectrum of m/z 345 was identical to the MS^3 spectrum of m/z 345 of M3, suggesting that M8 was a glucuronide of M3. The proposed structure of M8 is shown in Figure 6.

Oxidative Metabolism of PF-04971729 by Recombinant Human CYP Enzymes. In order to identify the human CYP isozyme(s) responsible for the metabolism of PF-04971729, PF-04971729 (20 μM) was incubated in NADPH-supplemented cDNA-expressed CYP isozymes CYP1A2, CYP2D6, CYP2C9, CYP2C19, CYP2E1, CYP3A4 and CYP3A5 at 37 ^oC for 1 h.

DMD Fast Forward. Published on June 20, 2011 as DOI: 10.1124/dmd.111.040675
This article has not been copyedited and formatted. The final version may differ from this version.

LC-MS/MS analysis indicated that CYP3A4/3A5 were the principle enzymes responsible for the biotransformation of PF-04971729 to metabolites M1 – M4 (Figure 8). Trace amounts of M2 were also in recombinant CYP2D6 incubations of PF-04971729.

Glucuronidation of PF-04971729 by Recombinant Human UGT Enzymes. In order to identify the human UGT isozyme(s), which were responsible for the glucuronidation of PF-04971729, PF-04971729 (20 μM) was incubated in UDPGA-supplemented recombinant UGT isozymes (UGT1A1, 1A3, 1A4, 1A6, 1A8, 1A9, 1A10, 2B4, 2B7 and 2B15) at 37 ^{o}C for 40 min. Amongst the panel of UGT enzymes evaluated, only UGT1A9 and UGT2B7 catalyzed the glucuronidation of PF-04971729 to M5 regioisomers (see Figure 8).

Human Pharmacokinetic Projections. A single species allometric scaling approach (Hosea *et al.* 2009, Frederick et al., 2009) of rat CL_p and Vd_{ss} values (normalized for protein binding) was used to project human clearance and volume. This exercise led to a predicted low CL_p (i.v. clearance = 1.7 ml/min/kg and p.o. clearance = 2.6 ml/min/kg) and moderate Vd_{ss} value of 1.8 l/kg for PF-04971729 in humans. The half-life of PF-04971729 in humans as derived from the equation $T_{1/2} = 0.693 \times Vd_{ss} / CL_p$ was estimated to be ~ 12 h. Extrapolation of oral bioavailability from rat to human, using single species allometry, provided an estimate of ~ 65%.

Single Dose Pharmacokinetics of PF-04971729 in humans. Following single oral dose administration to healthy volunteers, PF-04971729 was rapidly absorbed with mean plasma concentrations occurring at 0.5 to 1.5 hours postdose. Systemic exposure as ascertained from C_{max} and $AUC_{0-\infty}$ appeared to be dose-proportional over the dose range evaluated of PF-04971729 (0.5 – 300 mg) in healthy human volunteers (data not shown). The terminal half-life ($t_{1/2}$) of PF-04971729 was 11-17 hours and CL/F was within 1.5-fold of that predicted from single species allometric scaling.

DMD Fast Forward. Published on June 20, 2011 as DOI: 10.1124/dmd.111.040675
This article has not been copyedited and formatted. The final version may differ from this version.

Discussion

The pharmacokinetics of the potent and selective SGLT2 inhibitor, PF-04971729, in rats and dogs were characterized by low clearance (< 7 ml/min/kg) and a moderate steady state distribution volume (0.8 – 1.1 l/kg). Following p.o. administration as a methylcellulose/polyethylene glycol 400 suspension, PF-04971729 was rapidly absorbed in preclinical species with T_{max} values ~ 0.5 to 1 h. The fraction of the oral dose absorbed (F_a) in rat and dog was estimated using the equation $F_a = F/(1 - CL_b/Q)$. Using rat and dog hepatic blood flows of 70 and 35 ml/min/kg, F_a was estimated to be ~ 75% and ~ 100% for rats and dogs, respectively. Human oral F was predicted using rat F_a, assuming linear correlation between the oral fraction absorbed in rat and human (Chiou and Barve, 1998). Thus, using the rat F_a value of 0.75 and predicted human clearance of 1.7 ml/min/kg, the oral F of PF-04971729 in humans is anticipated to be ~ 65% (Chiou and Barve, 1998). As such, the oral F prediction for PF-04971729 is in agreement with the moderate absorptive permeability discerned in the Caco-2 assay. The BA/AB efflux ratio of 2.1, discerned in the Caco-2 permeability assay, suggests that PF-04971729 is potentially a substrate for efflux. However, the presence of the dual p-gp /BCRP inhibitor CP-100,356 did not greatly increase the absorptive permeability of PF-04971729. Although, the overall impact of efflux transport on oral absorption of PF-04971729 remains unclear, high oral F was observed in rats and dogs. Furthermore, because of the linear pharmacokinetic response in oral preclinical species toxicity evaluation and first-in-human studies (data not shown), it is unlikely that efflux plays an important role in the oral absorption of PF-04971729.

Consistent with the observed low in vivo CL_p, stability studies in liver microsomes and hepatocytes from preclinical species and human did not lead to significant compound turnover.

DMD Fast Forward. Published on June 20, 2011 as DOI: 10.1124/dmd.111.040675
This article has not been copyedited and formatted. The final version may differ from this version.

The inability to measure turnover of PF-04971729 in standard *in vitro* systems meant that traditional approaches of scaling *in vitro* intrinsic clearance data from human liver microsomes and hepatocytes to predict hepatic clearance *in vivo* could not be pursued for this compound. Consequently, a single-species scaling approach that previously has been shown to be successful for a large data set of proprietary compounds (Hosea *et al*. 2009, Frederick *et al.* 2009) was used to predict human clearance. The predicted human CL_p (i.v. = 1.7 ml/min/kg and p.o. = 2.6 ml/min/kg) and Vd_{ss} (1.8 l/kg) for PF-04971729 obtained from single species allometric scaling of rat pharmacokinetic data led to a predicted half-life of ~ 12 h in human. The observed *CL*/*F* of PF-04971729 in humans over the dose range examined was within 1.5-fold of the predicted value of 2.4 ml/min/kg. Likewise, the terminal half-life of 11 – 17 h in humans is in the vicinity of the predicted half-life of ~ 12 h. Overall, the oral pharmacokinetics of PF-04971729 in human was generally favorable as judged from the C_{max} and AUC, which increased in a dose-dependent fashion over the dose range examined.

Preliminary *in vitro* metabolite identification studies using a combination of liver microsomes and hepatocytes indicated that both phase I (CYP mediated oxidation) and phase II (UGT mediated conjugation) metabolic pathways contributed towards the biotransformation of PF-04971729. All metabolites detected in human *in vitro* systems were also observed in microsomes and hepatocytes from rat and dog, the preclinical species for toxicological evaluation. Studies in human hepatocytes indicated that glucuronidation of the glycosidic OH group(s) to the regioisomers M5b and M5c constituted the major metabolic fate of PF-04971729. Because PF-04971729 demonstrated no turnover in NADPH-supplemented human liver microsomes, preliminary reaction phenotyping was conducted using recombinant CYP enzymes. Results from this analysis revealed that oxidative metabolites of PF-04971729 were formed

principally through the catalytic action of CYP3A4/3A5 enzymes. Similar studies examining the role of UGT isoforms in the glucuronidation of PF-04971729 revealed that UGT1A9 and UGT2B7 isoforms played a role. The likelihood that PF-04971729 will undergo significant biliary excretion in humans appears to be low since studies addressing this clearance mechanism in bile-duct exteriorized rats revealed very little biliary excretion (< 5% of the administered dose) after i.v. administration of PF-04971729. Furthermore, analysis of human urine in the clinical study revealed that unchanged PF-04971729 in urine over 72 h accounted for ~ 1% of the p.o. dose (data not shown). This finding contrasts the observation in rats, wherein, ~ 27% of the i.v. dose of PF-04971729 was excreted in the urine in the parent form. Whether the differences in renal excretion profile in rats and humans are due to differences in substrate affinity of PF-04971729 towards organic anion transporters in the respective species needs to be investigated further.

From a drug-drug interaction standpoint, the finding that PF-04971729 was devoid of competitive or time-dependent inhibition of the catalytic activities of the major human CYP enzymes suggest that there is low potential for pharmacokinetic interaction of PF-04971729 with co-administered drugs that are metabolized by these CYP enzymes. Likewise, inhibitory effects against the human OCT2 transporter by PF-04971729 were weak (IC_{50} > 900 μM), and, at the unbound systemic exposures (free C_{max} = 1.0 – 11 nM) associated with efficacious daily doses of PF-04971729 (1.1 – 13 mg, Maurer et al., manuscript in preparation) are unlikely to cause pharmacokinetic interactions with the OCT2 substrate, metformin, a treatment of choice for T2DM (Setter et al, 2003). In the case of metformin, the principal clearance mechanism involves active renal excretion in the unchanged form, which is mediated by OCT2 (Kimura et al., 2005); modulation of this elimination mechanism through inhibition and/or genetic polymorphisms is

known to result in drug-drug interactions (Chen et al. 2009; Bachmakov et al., 2009). Finally, with the involvement of multiple elimination mechanisms (e.g., CYP3A4/3A5 and CYP2D6 oxidation and UGT1A9/2B7 glucuronidation) for PF-04971729, the fraction of drug metabolized via a single clearance pathway is reduced and so is the potential for pharmacokinetic interactions involving that pathway. From a drug safety perspective, PF-04971729 did not form glutathione conjugates (consistent with reactive metabolite formation) in NADPH- and glutathione-fortified human liver microsomes; therefore, PF-04971729 should not present a risk for immune-mediated toxicity due to reactive metabolite formation.

To conclude, the study provides important information pertaining to the disposition profile of PF-04971729, a novel and selective SGLT2 inhibitor, in preclinical species and human. A key highlight of this work was the ability to predict human pharmacokinetics with reasonable confidence using allometric scaling of *in vivo* data from a single animal species. The favorable absorption, distribution, metabolism and excretion characteristics and lack of drug-drug interaction concerns with PF-04971729 supported its progression into clinical trials.

DMD Fast Forward. Published on June 20, 2011 as DOI: 10.1124/dmd.111.040675
This article has not been copyedited and formatted. The final version may differ from this version.

Authorship Contributions.

Participated in research design: Kalgutkar, Tugnait, Zhu, Miao, Mascitti, Feng, and Robinson

Conducted experiments: Kimito, Miao, Yang, Tan, Walsky, and Chupka

Contributed new reagents or analytic tools: Mascitti, and Robinson

Performed data analysis: Kimito, Miao, Yang, Walsky, and Chupka

Wrote or contributed to the writing of the manuscript: Kalgutkar, Tugnait, and Zhu

DMD Fast Forward. Published on June 20, 2011 as DOI: 10.1124/dmd.111.040675
This article has not been copyedited and formatted. The final version may differ from this version.

References

Abdul-Ghani MA and DeFronzo RA (2008) Inhibition of renal glucose reabsorption: a novel strategy for achieving glucose control in type 2 diabetes mellitus. *Endocr Pract* **14:**782-790.

Adachi T, Yasuda K, Okamoto Y, Shihara N, Oku A, Ueta K, Kitamura K, Saito A, Iwakura I, Yamada Y, Yano H, Seino Y, and Tsuda K (2000) T-1095, a renal Na+-glucose transporter inhibitor, improves hyperglycemia in streptozotocin-induced diabetic rats. *Metabolism* **49:**990-995.

Aires I and Calado J (2010) BI-10773, a sodium-glucose cotransporter 2 inhibitor for the potential oral treatment of type 2 diabetes mellitus. *Curr Opin Investig Drugs* **11:**1182-1190.

Bachmakov I, Glaeser H, Endress B, Mörl F, König J and Fromm MF (2009) Interaction of beta-blockers with the renal uptake transporter OCT2. *Diabetes Obes Metab* **11:**1080-1083.

Bailey CJ, Gross JL, Pieters A, Bastien A, and List JF (2010) Effect of dapagliflozin in patients with type 2 diabetes who have inadequate glycaemic control with metformin: a randomized, double-blind, placebo-controlled trial. *Lancet* **375:**2223-2233.

Bołdys A and Okopień B (2009) Inhibitors of type 2 sodium glucose co-transporters--a new strategy for diabetes treatment. *Pharmacol Rep* **61:**778-784.

Chen Y, Li S, Brown C, Cheatham S, Castro RA, Leabman MK, Urban TJ, Chen L, Yee SW, Choi JH, Huang Y, Brett CM, Burchard EG, and Giacomini K (2009) Effect of genetic variation in the organic cation transporter 2 on the renal elimination of metformin. *Pharmacogenet Genomics* **19:**497-504.

Chiou WL and Barve A (1998) Linear correlation of the fraction of oral dose absorbed of 64 drugs between humans and rats. *Pharm Res* **15:**1792-1795.

DeFronzo RA (1988) Lilly Lecture: The triumvirate: β-cell, muscle, liver: a collusion responsible for NIDDM. *Diabetes* **37:**667–687.

DeFronzo RA (2009) Banting Lecture. From the triumvirate to the ominous octet: a new paradigm for the treatment of type 2 diabetes mellitus. *Diabetes* **58:**773-795.

Elsby R, Surry DD, Smith VN, and Gray AJ (2008) Validation and application of Caco-2 assays for the in vitro evaluation of development candidate drugs as substrates or inhibitors of P-glycoprotein to support regulatory submissions. *Xenobiotica,* 38:1140-1164.

Frederick KS, Maurer TS, Kalgutkar AS, Royer LJ, Francone OL, Winter SM, Terra SG, Chen D, and Gao X (2009) Pharmacokinetics, disposition and lipid-modulating activity of 5-{2-[4-(3,4-difluorophenoxy)-phenyl]-ethylsulfamoyl}-2-methyl-benzoic acid, a potent and subtype-selective peroxisome proliferator-activated receptor α agonist in preclinical species and human. *Xenobiotica* **39:**766-781.

Fujimori Y, Katsuno K, Nakashima I, Ishikawa-Takemura Y, Fujikura H, and Isaji M (2008) Remogliflozin etabonate, in a novel category of selective low-affinity sodium glucose cotransporter (SGLT2) inhibitors, exhibits antidiabetic efficacy in rodent models. *J Pharmacol Exp Ther* **327:**268-276.

Hosea NA, Collard WT, Cole S, Maurer TS, Fang RX, Jones H, Kakar SM, Nakai Y, Smith BJ, Webster R, and Beaumont K (2009) Prediction of human pharmacokinetics from preclinical information: comparative accuracy of quantitative prediction approaches. *J Clin Pharmacol* **49:**513-533.

Kasichayanula S, Chang M, Hasegawa M, Liu X, Yamahira N, LaCreta FP, Imai Y, and Boulton DW. (2011) Pharmacokinetics and pharmacodynamics of dapagliflozin, a novel selective

inhibitor of sodium-glucose co-transporter type 2, in Japanese subjects without and with type 2 diabetes mellitus. *Diabetes Obes. Metab* **13:**357-365.

Kalgutkar AS, Frederick KS, Chupka J, Feng B, Kempshall S, Mireles RJ, Fenner KS, and Troutman MD (2009) N-(3,4-Dimethoxyphenethyl)-4-(6,7-dimethoxy-3,4-dihydroisoquinolin-2[1H]-yl)-6,7-dimethoxyquinazolin-2-amine (CP-100,356) as a "chemical knock-out equivalent" to assess the impact of efflux transporters on oral drug absorption in the rat. *J Pharm Sci* **98:**4914-4927.

Kanai Y, Lee WS, You G, Brown D, and Hediger MA (1994) The human kidney low affinity Na+/glucose cotransporter SGLT2. Delineation of the major renal reabsorptive mechanism for D-glucose. *J Clin Invest* **93:**397-404.

Katsuno K, Fujimori Y, Takemura Y, Hiratochi M, Itoh F, Komatsu Y, Fujikura H, and Isaji M (2007) Sergliflozin, a novel selective inhibitor of low-affinity sodium glucose cotransporter (SGLT2), validates the critical role of SGLT2 in renal glucose reabsorption and modulates plasma glucose level. *J Pharmacol Exp Ther* **320:**323-330.

Kimura N, Masuda S, Tanihara Y, Ueo H, Okuda M, Katsura T, and Inui K (2005) Metformin is a superior substrate for renal organic cation transporter OCT2 rather than hepatic OCT1. *Drug Metab Pharmacokinet* **20:**379-386.

King H, Aubert RE, and Herman WH (1998) Global burden of diabetes, 1995-2025: prevalence, numerical estimates, and projections. *Diabetes Care* **21:**1414-1431.

List JF, Woo V, Morales E, Tang W, and Fiedorek FT (2009) Sodium-glucose cotransport inhibition with dapagliflozin in type 2 diabetes. *Diabetes Care* **32:**650-657.

Mascitti V, Maurer TS, Robinson RP, Bian J, Boustany-Kari CM, Brandt T, Collman BM, Kalgutkar AS, Klenotic MK, Leininger MT, Lowe A, Maguire RJ, Masterson VM, Miao Z,

Mukaiyama E, Patel JD, Pettersen JC, Préville C, Samas B, She L, Sobol Z, Steppan CM, Stevens BD, Thuma BA, Tugnait M, Zeng D, and Zhu T.(2011) Discovery of a Clinical Candidate from the Structurally Unique Dioxa-bicyclo[3.2.1]octane Class of Sodium-Dependent Glucose Cotransporter 2 Inhibitors. *J Med Chem* **54:**2952-2960.

Meng W, Ellsworth BA, Nirschl AA, McCann PJ, Patel M, Girotra RN, Wu G, Sher PM, Morrison EP, Biller SA, Zahler R, Deshpande PP, Pullockaran A, Hagan DL, Morgan N, Taylor JR, Obermeier MT, Humphreys WG, Khanna A, Discenza L, Robertson JG, Wang A, Han S, Wetterau JR, Janovitz EB, Flint OP, Whaley JM, and Washburn WN (2008) Discovery of dapagliflozin: a potent, selective renal sodium-dependent glucose cotransporter 2 (SGLT2) inhibitor for the treatment of type 2 diabetes. *J Med Chem* **51:**1145-1149.

Mokdad AH, Ford ES, Bowman BA, Dietz WH, Vinicor F, Bales VS and Marks JS (2003) Prevalence of obesity, diabetes, and obesity-related health risk factors, 2001. *JAMA* **289:**76-79.

Nair S and Wilding JP (2010) Sodium glucose cotransporter 2 inhibitors as a new treatment for diabetes mellitus. *J Clin Endocrinol Metab* **95:**34-42.

Neumiller JJ, White JR Jr, and Campbell RK (2010) Sodium-glucose co-transport inhibitors: progress and therapeutic potential in type 2 diabetes mellitus. *Drugs* **70:**377-385.

Oku A, Ueta K, Arakawa K, Ishihara T, Nawano M, Kuronuma Y, Matsumoto M, Saito A, Tsujihara K, Anai M, Asano T, Kanai Y, and Endou H (1999) T-1095, an inhibitor of renal Na^+-glucose cotransporters, may provide a novel approach to treating diabetes. *Diabetes* **48:**1794-1800.

Pacifici GM and Viani A (1992) Methods of determining plasma and tissue binding of drugs. *Clinical Pharmacokinetics* **23:**449-468.

Pajor AM and Wright EM (1992) Cloning and functional expression of a mammalian Na+/nucleoside cotransporter. A member of the SGLT family. *J Biol Chem* **267:**3557-3560.

Robinson RP, Mascitti V, Boustany-Kari CM, Carr CL, Foley PM, Kimoto E, Leininger MT, Lowe A, Klenotic MK, Macdonald JI, Maguire RJ, Masterson VM, Maurer TS, Miao Z, Patel JD, Préville C, Reese MR, She L, Steppan CM, Thuma BA, and Zhu T (2010) C-Aryl glycoside inhibitors of SGLT2: Exploration of sugar modifications including C-5 spirocyclization. *Bioorg Med Chem Lett* **20:**1569-1572.

Setter SM, IItz JL, Thams J, and Campbell RK (2003) Metformin hydrochloride in the treatment of type 2 diabetes mellitus: a clinical review with a focus on dual therapy. *Clin Ther* **25:**2991-3026.

Sha S, Devineni D, Ghosh A, Polidori D, Chien S, Wexler D, Shalayda K, Demarest K, and Rothenberg P. (2011) Canagliflozin, a novel inhibitor of sodium glucose co-transporter 2, dose-dependently reduces calculated renal threshold for glucose excretion and increases urinary glucose excretion in healthy subjects. *Diabetes Obes Metab* In Press.

Stratton IM, Adler AI, Neil HA, Matthews DR, Manley SE, Cull CA, Hadden D, Turner RC and Holman RR (2000) Association of glycaemia with macrovascular and microvascular complications of type 2 diabetes (UKPDS 35): prospective observational study. *British Med J* **321:**405-412.

Wallner EI, Wada J, Tramonti G, Lin S, and Kanwar YS (2001) Status of glucose transporters in the mammalian kidney and renal development. *Ren Fail* **23:**301-310.

Walsky RL and Obach RS (2004) Validated assays for human cytochrome P450 activities. *Drug Metab Dispos* **32:**647-660.

Wilding JP, Norwood P, T'joen C, Bastien A, List JF, and Fiedorek FT (2009) A study of dapagliflozin in patients with type 2 diabetes receiving high doses of insulin plus insulin sensitizers: applicability of a novel insulin-independent treatment. *Diabetes Care* **32:**1656-1662.

Wright EM (2001) Renal Na(+)-glucose cotransporters. *Am J Physiol Renal Physiol* 280:F10-18.

Zhang X, Urbanski M, Patel M, Zeck RE, Cox GG, Bian H, Conway BR, Pat Beavers M, Rybczynski PJ, and Demarest KT (2005) Heteroaryl-O-glucosides as novel sodium glucose co-transporter 2 inhibitors. Part 1. *Bioorg Med Chem Lett* **15:**5202-5206.

Zhang X, Urbanski M, Patel M, Cox GG, Zeck RE, Bian H, Conway BR, Beavers MP, Rybczynski PJ, and Demarest KT (2006) Indole-glucosides as novel sodium glucose co-transporter 2 (SGLT2) inhibitors. Part 2. *Bioorg Med Chem Lett* **16:**1696-1701.

Zolk O, Solbach TF, König J, and Fromm MF (2009) Structural determinants of inhibitor interaction with the human organic cation transporter OCT2 (*SLC22A2*). *Naunyn-Schmied Arch Pharmacol* **379:**337-348.

DMD Fast Forward. Published on June 20, 2011 as DOI: 10.1124/dmd.111.040675
This article has not been copyedited and formatted. The final version may differ from this version.

Figure Legends

FIG. 1. Structure of PF-04971729.

FIG. 2. Inhibition of hOCT2-mediated uptake of [^{14}C]-metformin by PF-04971729. The net uptake values were obtained by subtracting the uptake in vector-transfected cells (control) from those in OCT2-expressing cells. The net uptake without inhibitor was defined as 100%. The IC_{50} value for PF-04971729 was estimated from a semi-logarithmic plot of concentrations versus percentage of net uptake relative to the control. Each value represents the mean ± S.D. (n = 3).

FIG. 3. Concentrations of PF-04971729 in plasma of rats (A), dogs (B) after intravenous and oral administration. Each point represents the mean of two or three determinations.

FIG. 4. Extracted ion chromatograms of incubation mixtures of PF-04971729 (10 μM) in NADPH-supplemented liver microsomes from rat (A), dog (B) and human (C).

FIG. 5. CID spectrum of PF-04971729. Panel A represents the MS^2 spectrum of $(M + NH_4)^+$ = 454 and panel B depicts the MS^3 spectrum of $(m/z + H)^+$ = 329.

FIG. 6. Proposed structures and assignments of MS fragmentation pattern for the metabolites of PF-04971729 in liver microsomes and hepatocytes from rat, dog and human.

FIG. 7. Extracted ion chromatograms of incubation mixtures of PF-04971729 (10 μM) in cryopreserved hepatocytes from rat (A), dog (B) and human (C).

FIG. 8. Extracted ion chromatograms of incubation mixtures of PF-04971729 (20 μM) in recombinant human CYP3A4 (A), CYP3A5 (B), UGT1A9 (C) and UGT2B7 (D).

TABLE 1

Pharmacokinetic parameters of PF-04971729 in rats and dogs following a single i.v. or p.o. dose

Species (strain)	Gender/n	Dose[a]	Route	C_{max}	T_{max}	CL_p	Vd_{ss}	$AUC_{(0-\infty)}$	$T_{1/2}$	*F*
		mg/kg		ng/ml	h	ml/min/kg	l/kg	ng.hr/ml	h	%
Rat (Sprague-Dawley)	M/2	2.0	i.v.	NA	NA	4.04 (3.39,4.68)	1.13 (1.18,1.08)	8480 (9830,7040)	4.08 (4.85,3.31)	NA
	M/3	5.0	p.o.	1940±185	1.0±0.0	NA	NA	14700±4320[b]	NA	69
Dog (Beagle)	M/2	2.0	i.v.	NA	NA	1.64 (1.72,1.56)	0.83 (0.81,0.84)	20400 (19400,21400)	7.63 (7.42,7.84)	NA
	M/3	2.0	p.o.	2500±215	0.83±0.29	NA	NA	19100±365	7.48±0.13	94

NA, not applicable.

[a]Dosing vehicle used in i.v. and p.o. dosing to rats was DMSO/polyethylene glycol 400/30% sulfobutylether-β-Cyclodextrin (10/30/60, v/v/v) and 0.5% (w/v) methyl cellulose with 10% (v/v) polyethylene glycol 400. Dosing vehicle used in i.v. and p.o. dosing to dogs was 5% polyethylene glycol 400 in 23% hydroxypropyl-β-cyclodextrin and 0.5% methyl cellulose (w/v) with 10% (v/v) polyethylene glycol 400, respectively.

[b]$AUC_{(0-24)}$.

DMD Fast Forward. Published on June 20, 2011 as DOI: 10.1124/dmd.111.040675
This article has not been copyedited and formatted. The final version may differ from this version.

TABLE 2

LC-MS data for 1 and its metabolites (M1 – M7) in liver microsomes and cryopreserved hepatocytes from rat, dog and human

Compound	t_R (min)[a]	Observed ($(M+NH_4)^+$)[b]	LC-MS*n* fragments, m/z
M6a	11.6	602.16404	MS^2 on m/z 602.16404: 409.1049, 301.0626, 207.0207; MS^3 on *m/z* 602 → 409: 301.0626, 207.0207, 107.0491
M7	11.9	442.12	MS^2 on m/z 442.12: 424/37, 397.19, 299.08, 271.20
M6b	12.2	602.16401	MS^2 on m/z 602.16401: 409.1049, 301.0626, 207.0207; MS^3 on *m/z* 602 → 409: 301.0626, 207.0207, 107.0491
M6c	12.3	602.16402	MS^2 on m/z 602.16402: 409.1049, 301.0626, 207.0207; MS^3 on *m/z* 602 → 409: 301.0626, 207.0207, 107.0491
M8	13.9	646.19	MS^2 on *m/z* 646.19: 470.06, 453.12, 345.04, 207.14; MS^3 on *m/z* 426 → 453: 345, 297; MS^4 on *m/z* 453 → 345: 207, 151, 139, 123
M2	15.9	426.1320	MS^2 on *m/z* 426.1320: 409.1050, 301.0626; MS^3 on *m/z* 426 → 409: 301.0628; MS^4 on m/z 426 → 409 → 301: 207.0208, 107.4914
M1	17.3	470.1580	MS^2 on *m/z* 470.1580: 435.1204; MS^3 on *m/z* 470 → 435: 407.0891, 299.0470, 243.0209
M3	18.1	470.1583	MS^2 on *m/z* 470.1583: 453.1311, 345.0889, 207.0206, 151.0755; MS^3 on *m/z* 470 → 435: 207.0208, 151.0754, 139.0754, 123.0440
M5a	18.7	630.1952	MS^2 on *m/z* 630.1952: 437.1362, 329.0940, 135.082
M5b	19.1	630.1954	MS^2 on *m/z* 630.1954: 437.1362, 329.0940, 135.0802
M4	20.1	470.15	MS^2 on *m/z* 470.15: 435.0; MS^3 on *m/z* 470 → 435: 417.1, 369.1, 329.0, 207.1, 135.1
M5c	20.6	630.1953	MS^2 on *m/z* 630.1953: 437.1362, 329.0940, 135.0802
PF-04971729	31.0	454.1632	MS^2 on *m/z* 454.1632: 437.1359; 329.0939; MS^3 on *m/z* 454 → 329: 273.0677, 207.0206, 135.0802

[a]Under HPLC conditions listed in the materials and methods section.

DMD Fast Forward. Published on June 20, 2011 as DOI: 10.1124/dmd.111.040675
This article has not been copyedited and formatted. The final version may differ from this version.

[b]Accurate mass data for PF-04971729 and its metabolites was generated using Orbitrap MS.

Figure 1

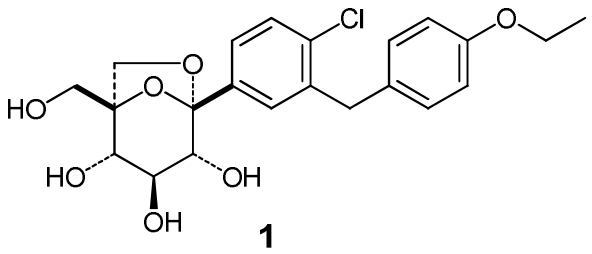

1

Figure 2

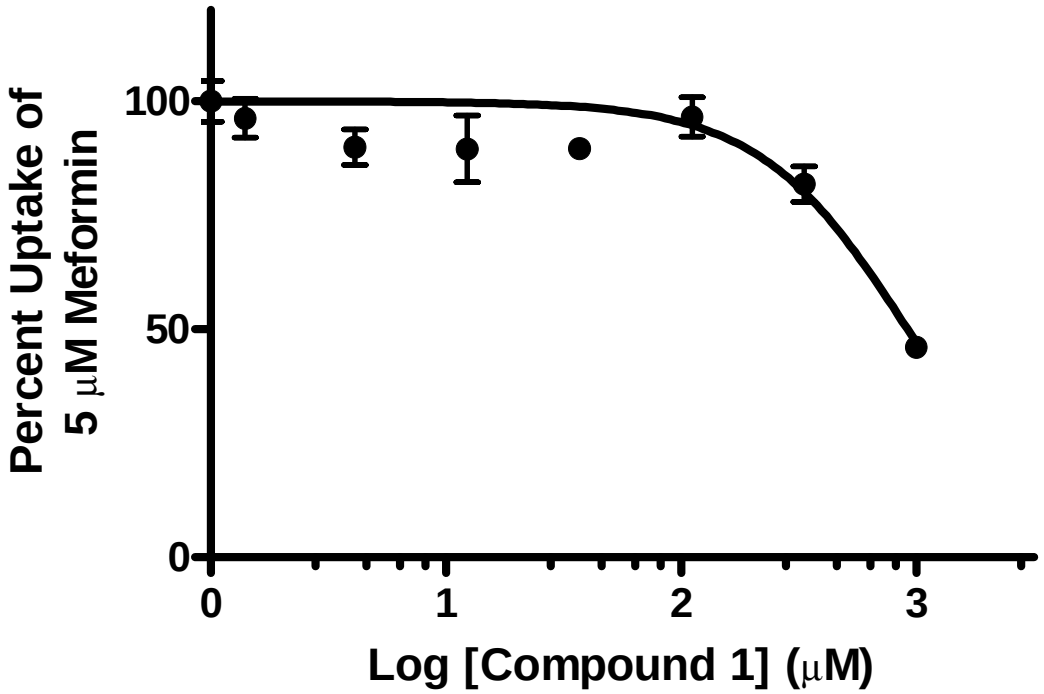

Figure 3

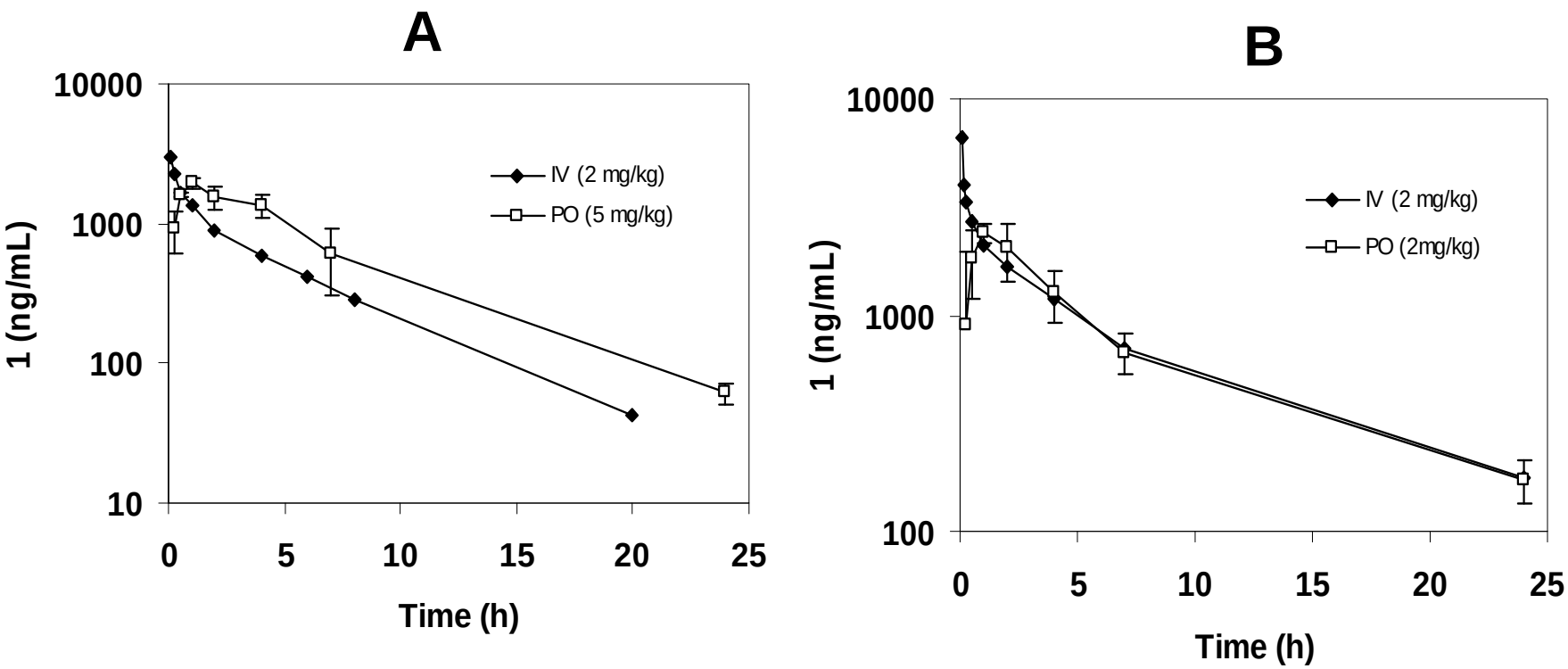

Figure 4

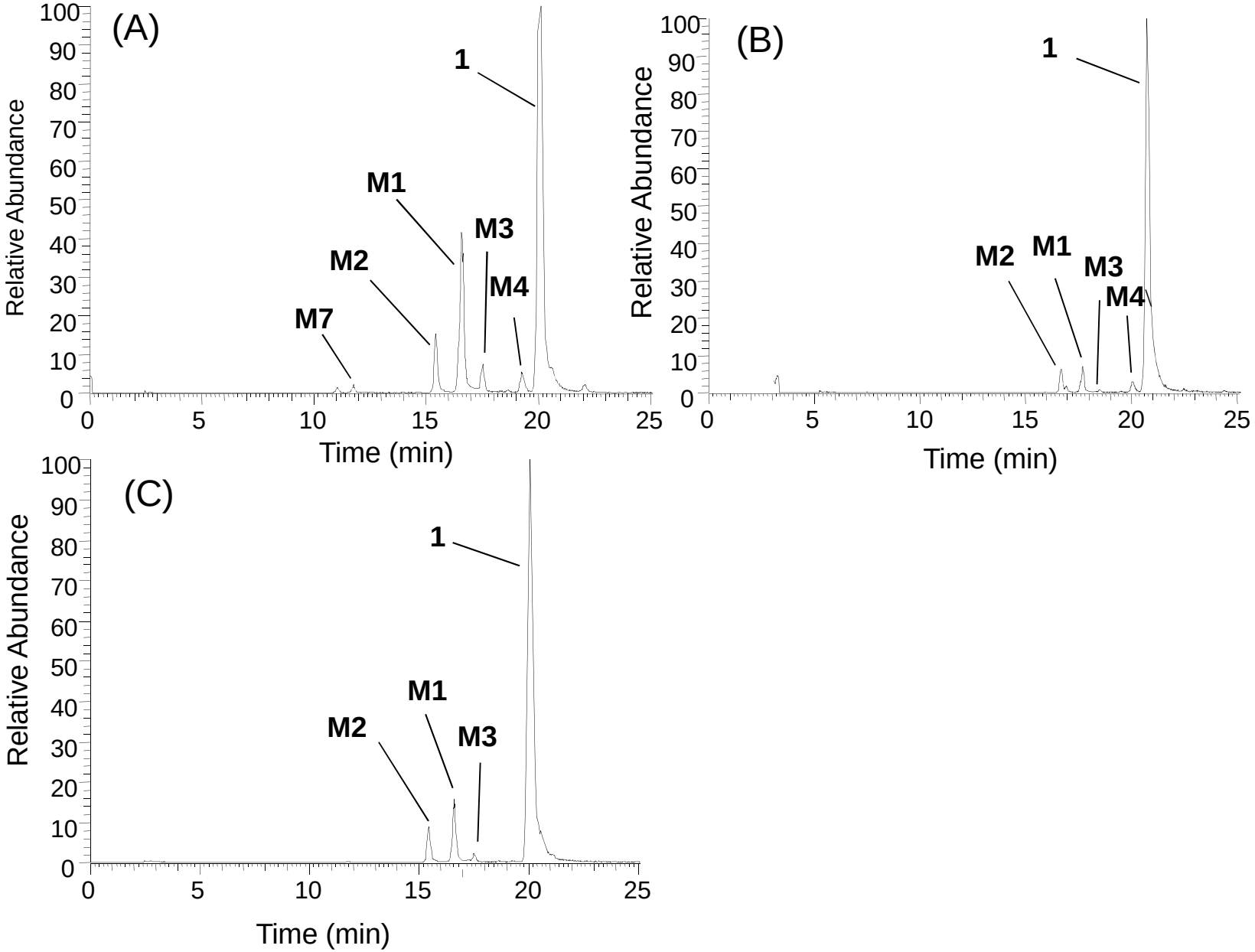

Figure 5

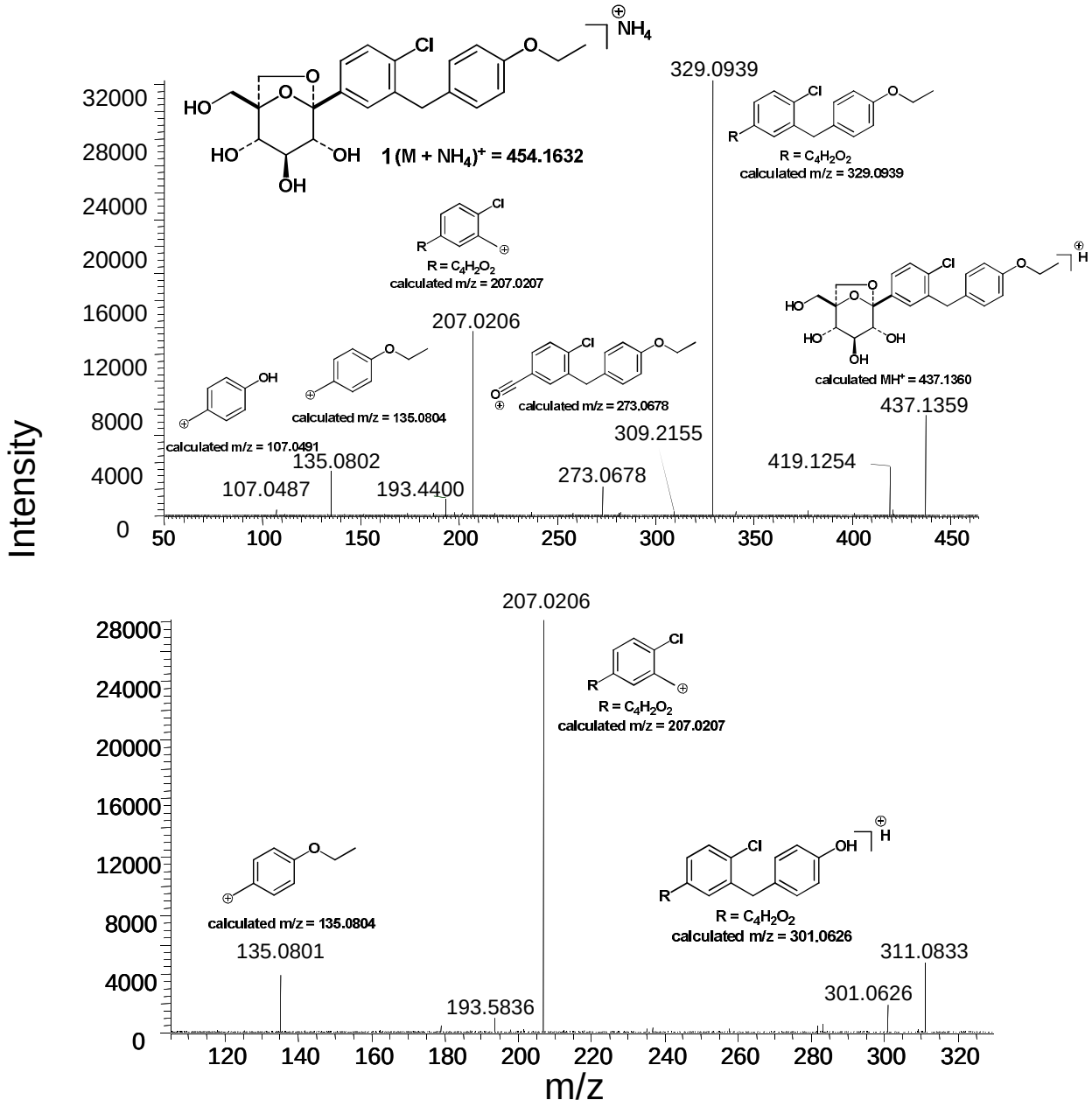

Figure 6

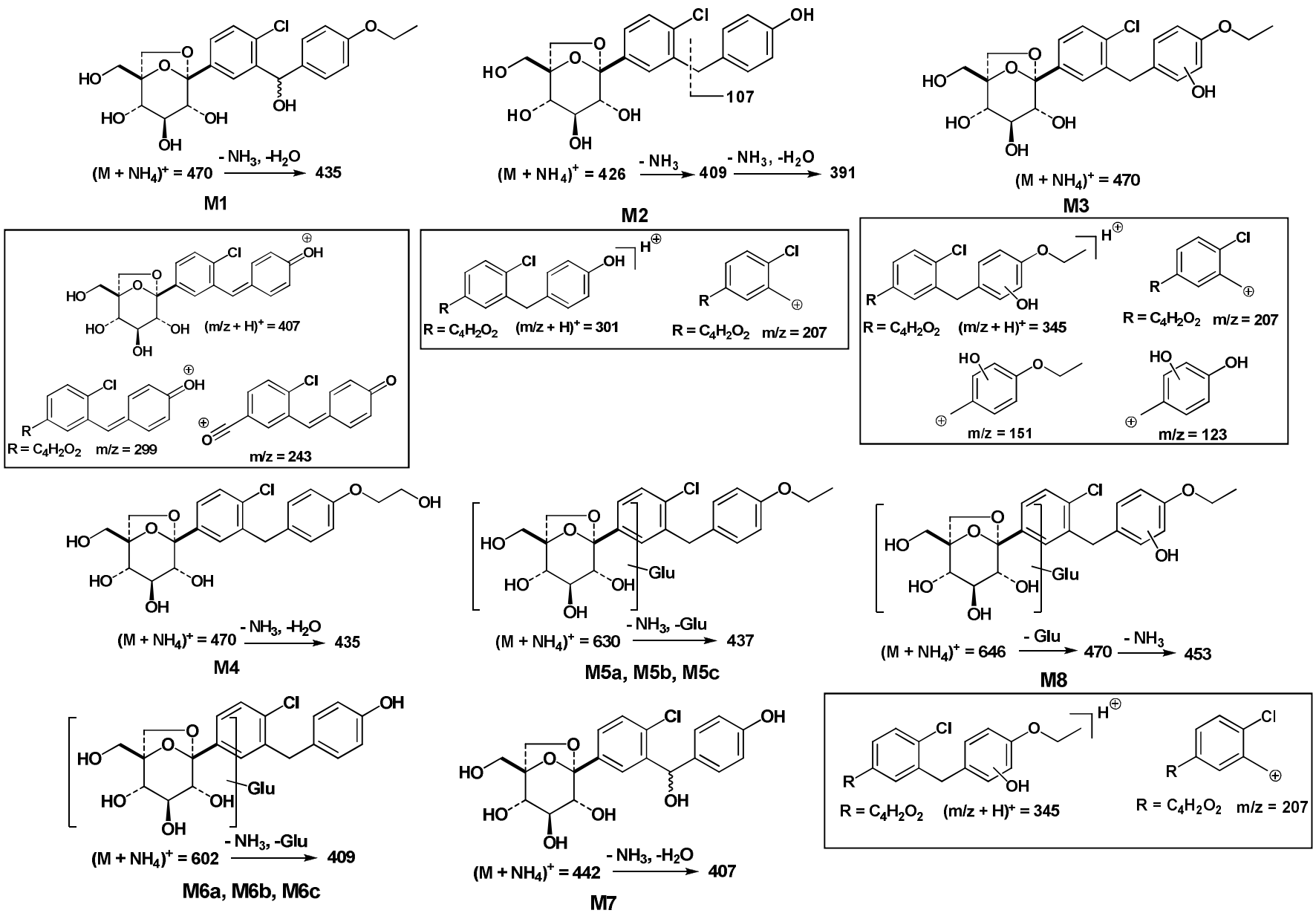

Figure 7

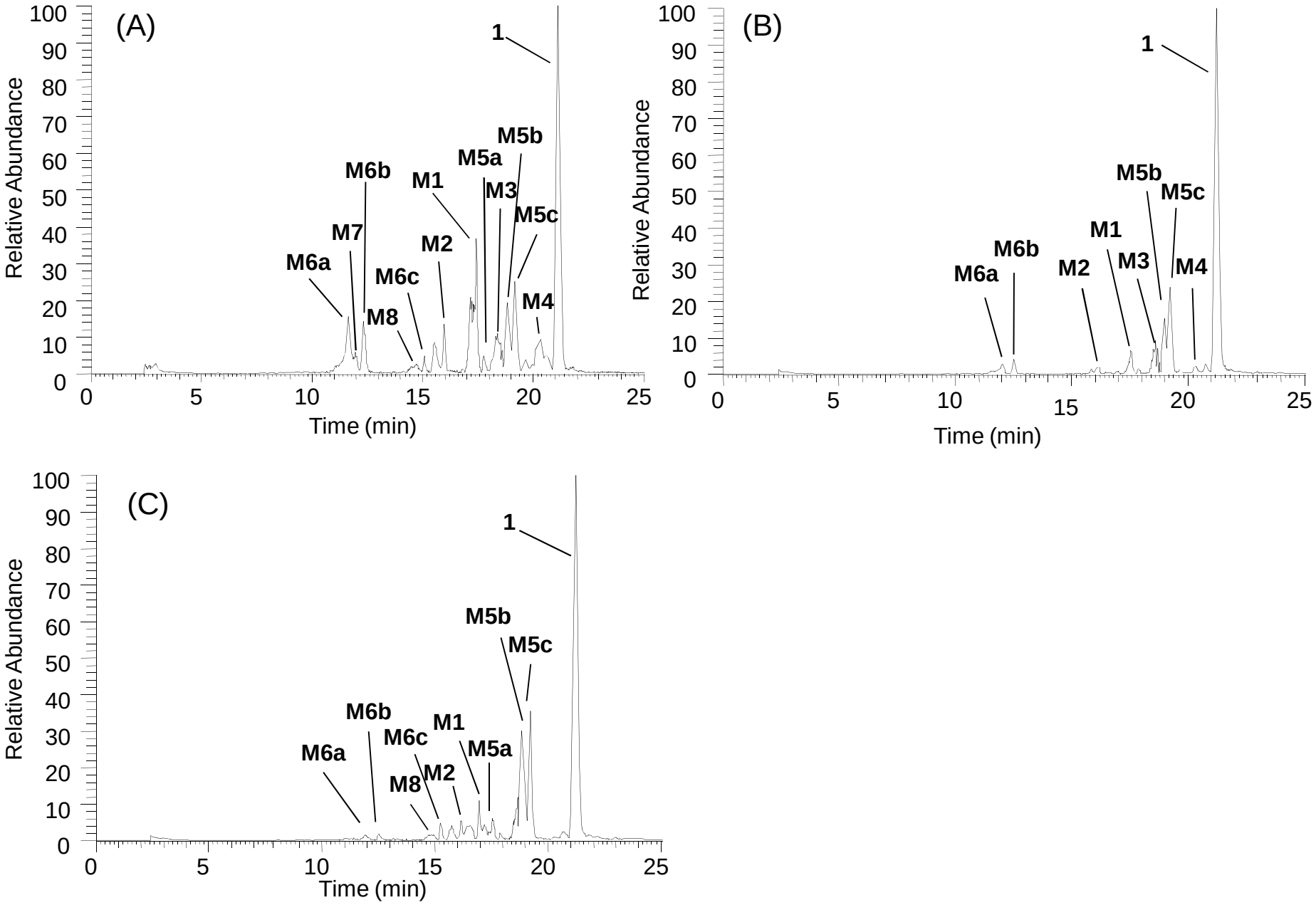

Figure 8